

# Deploying Four-Connectivity And Full-Coverage Wireless Sensor Networks

Xiaole Bai\*, Ziqiu Yun<sup>†</sup>, Dong Xuan\*, Ten H. Lai\* and Weijia Jia<sup>‡</sup>

\*Department of Computer Science and Engineering  
The Ohio State University, Columbus, OH 43210, USA  
Email: {baixia, xuan, lai}@cse.ohio-state.edu

<sup>†</sup>Department of Mathematics  
Suzhou University, Suzhou, 215006, P. R. China

Email: yunziqiu@public1.sz.js.cn

<sup>‡</sup>Department of Computer Science  
City University of Hong Kong, Hong Kong, P. R. China  
Email: wei.jia@cityu.edu.hk

**Abstract**—We study the issue of optimal deployment to achieve four connectivity and full coverage for wireless sensor networks (WSNs) under different ratios of sensors’ communication range (denoted by  $r_c$ ) to their sensing range (denoted by  $r_s$ ). We propose a “Diamond” pattern, which can be viewed as a series of different evolving patterns. When  $r_c/r_s \geq \sqrt{3}$ , the Diamond pattern coincides with the well-known triangle lattice pattern; when  $r_c/r_s \leq \sqrt{2}$ , it degenerates to a “Square” pattern. We prove the Diamond pattern to be asymptotically optimal when  $r_c/r_s > \sqrt{2}$ . Our work is the first to propose an asymptotically optimal deployment pattern to achieve four connectivity and full coverage for WSNs. We hope our work will provide some insights on how optimal patterns evolve and how to search for them.

## I. INTRODUCTION

Deployment is an important issue in wireless sensor networks (WSNs). There are two categories of deployment methods. One is random deployments; the other, planned deployments. With planned deployments, sensors are placed at planned, pre-determined locations. In planning where to deploy sensors, it is often desirable that the pattern will be such that the minimum number of sensors are needed. Aside from the theoretical interest, finding the optimal development pattern (in terms of number of sensors) has its practical significance. First, sensor nodes still cost close to \$100 a piece. Deploying the minimum number of sensors needed certainly is most desirable for the obvious economic reason. Second, insights obtained from optimal deployment patterns can be used to guide the development of heuristic algorithms for topology control [7], as well as to measure the relative performance of these heuristics as compared to the optimal one [13].

This work was supported in part by the US National Science Foundation (NSF) CAREER Award CCF-0546668, the Army Research Office (ARO) under grant No. AMSRD-ACC-R 50521-CI, NSFC grant No. 10571151 and SAR Hong Kong RGC Competitive Earmarked Research Grant (CERG) No. 9041129 (CityU 113906). Any opinions, findings, conclusions, and recommendations in this paper are those of the authors and do not necessarily reflect the views of the funding agencies.

However, finding optimal patterns for WSNs is a hard problem, and very few results on optimal patterns are available in the literature. For many years, the only result known to us on this topic had been a theorem proved in 1939, which states that regular triangular lattice pattern (triangle pattern in short) is asymptotically optimal in terms of number of circles needed to entirely cover a given area in the plane [8]. This result, formulated as one for sensor deployment, was proved again in [13] using a different method. In many applications of WSNs, it is not only required that sensors cover an entire area, but also that the sensors form a connected communication network. When both coverage and connectivity are required, the triangle pattern remains optimal when  $r_c/r_s \geq \sqrt{3}$ , where  $r_c$  and  $r_s$  are communication range and sensing range of sensors, respectively. In practice, the value of  $r_c/r_s$  has a wide range, not necessarily greater than  $\sqrt{3}$ . For example, while the reliable communication range of the Extreme Scale Mote (XSM) platform is 30m, the sensing range of the acoustics sensor for detecting an All Terrain Vehicle is 55m [1], in which case,  $r_c/r_s = 30/55 \ll \sqrt{3}$ . This has incited researchers’ interests to find an optimal deployment pattern to achieve both coverage and connectivity for a complete range of  $r_c/r_s$ . In 2005, a strip-based pattern was proposed that can achieve both coverage and connectivity, but without any study on its optimality [12]. That pattern was later independently described and proved to be near-optimal when  $r_c/r_s = 1$  [7]. In 2006, the strip-based pattern was proved to be not only near-optimal but actually asymptotically optimal; and not only for  $r_c/r_s = 1$ , but for all values of  $r_c/r_s$  [2]. The connectivity considered in these results is the simple 1-connectivity. Should connectivity of a higher degree be desired, a variant of the strip-based pattern was proved to be asymptotically optimal that achieves *two* connectivity and full coverage, again for all values of  $r_c/r_s$  [2].

A two-connected wireless sensor network is definitely more reliable in communication than a network which is just one-connected. But unfortunately, the aforementioned strip-based

pattern suffers a “long communication path” problem and, besides, two-connectivity is still deemed insufficient in many applications. The long communication path problem can be easily explained using a diagram. In Fig. 1, we depict the communication network of the two-connected strip-based pattern [2]. In the figure, note that even though nodes  $A$  and  $B$  are close to each other, they have to communicate, e.g., for the local data aggregation purpose, through a long multi-hop path. This results in long delay and waste of energy, which is a critical and rare resource in WSNs.

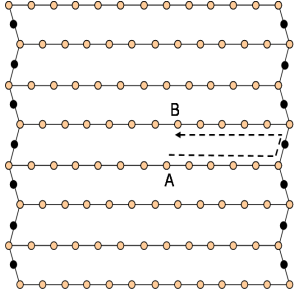


Fig. 1. An example to show the long communication path problem in the two connected strip-based pattern. Node  $A$  has to communicate through a long multi-hop path (in dash line) to reach Node  $B$  although they are close to each other.

Now, if two-connectivity is not sufficient, how much connectivity is necessary? Intuitively, with sensors deployed over a region in the plane, we would like each sensor (except for those near the boundaries) to be able to send messages directly up, down, left and right to an immediate neighbor, thereby avoiding the long communication path problem. This seems to suggest the requirement of four-connectivity. As a matter of fact, several research projects (e.g., data segmentation [9], routing [5], and storage [4] etc.) have assumed four-connectivity on their wireless sensor networks, a clear endorsement to the candidacy of four-connectivity.

This motivates us to investigate the problem of finding an optimal deployment pattern that achieves four connectivity and full coverage. As it turns out, there is no single pattern which is optimal for all values of  $r_c/r_s$ . This is in contrast to the case of two-connectivity (and full coverage), for which the strip-based pattern as mentioned above is optimal for all values of  $r_c/r_s$ . Our results are summarized as follows:

- We propose a “Diamond” pattern, which can be viewed as a series of different evolving patterns. When  $r_c/r_s \geq \sqrt{3}$ , the Diamond pattern coincides with the well-known triangle lattice pattern; when  $r_c/r_s \leq \sqrt{2}$ , it degenerates to a “Square” pattern.
- We prove the Diamond pattern to be asymptotically optimal when  $r_c/r_s > \sqrt{2}$ .
- Our search for optimal deployment patterns is not based on an ad hoc method. Rather, it is systematic, based on some mathematical theory. Doing so, we hope to shed some insights on how to search for optimal deployment patterns for WSNs.

The rest of the paper is organized as follows. In Section

II, we give the definitions and assumptions used throughout the paper. In Section III, we discuss our exploration on the optimal deployment pattern to achieve four-connectivity and full coverage. In Section IV, we discuss the evolution of deployment patterns. In Section V, we compute the number of nodes needed when different patterns are used. We discuss the non-disk sensing and communication models in Section VI. Section VII concludes the paper.

## II. PRELIMINARY

In this section, we present the preliminaries for our optimal deployment pattern exploration.

We assume that both the sensing and the communication scopes are disks, even though in reality the sensing and the communication ranges are likely to be non-isotropic or even roughly conform to a normal distribution probability model along each direction [15], [14], [3]. This is because results obtained with the simple disk model are still useful in many applications, and it has been adopted in a great amount of literatures, e.g., in [7], [13], [2]. Furthermore, abstractions are inevitable in order to achieve enough generality when we are trying to lay down certain theoretical foundations. More discussion on non-disk sensing and communication models is presented in Section VI.

Let  $r_s$  denote the sensing radius, and  $r_c$  the communication radius. The sensors are assumed to be homogeneous on their sensing range and communication range. We also assume that only one sensor can be deployed at one location.

This paper studies “asymptotically optimal” deployment patterns to achieve four-connectivity and full coverage. A deployment pattern is said to be *asymptotically optimal* if the pattern is optimal when the deployment area is fixed and the sensing range approaches zero, or equivalently, when sensing range is fixed and the deployment area approaches infinity. Informally, it means that the pattern is optimal if the deployment area is so large compared to the sensing range that we can ignore the boundary of the deployment area and consider only the interior nodes. If boundaries are not ignored, very few can be said about optimal deployment patterns. A pattern which is optimal for a region may not be optimal for another region (of a different shape or different area).

*Definition 1: Voronoi Polygon:* Let  $P = \{a_1, a_2, \dots, a_p\}$  be a set of  $p$  points on an Euclidean plane  $S$ . The Voronoi polygon  $V(a_i)$  is the set of all points in  $S$  which are closer to  $a_i$  (in terms of Euclidean distance) than to any other point in  $P$ , i.e.

$$V(a_i) := \{x \in S : \forall a_j \in P, d(x, a_i) \leq d(x, a_j)\}.$$

*Definition 2: Interior Node:* a node whose Voronoi polygon has no edge on the boundary of the deployment area.

*Definition 3: Four-connected Sensor Network:* A sensor network  $N$  is said to be four-connected if for every two interior nodes of  $N$  there are at least four node-disjoint paths joining them.

Note that in a full-coverage deployment, each Voronoi polygon corresponding to an interior sensor node is enclosed

in a sensing disk. Thus, as illustrated in Fig. 2(a), each edge of the Voronoi polygon resides on a common chord between two sensing disks. The common chord that contains an edge of a Voronoi polygon is said to be an *edge-chord*. For instance, in Fig. 2(b), the edge  $a'b'$  of the Voronoi polygon resides on the chord  $ab$ . Thus, chord  $ab$  is the edge-chord of edge  $a'b'$ .

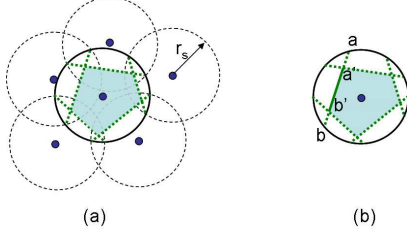


Fig. 2. The solid and dashed circles denote sensing disks. The shaded area denotes the Voronoi polygon of a sensor, which is shown as a dark dot. (a) In a full coverage deployment each Voronoi polygon is constructed by common chords of intersecting sensing disks. (b) Chord  $ab$  is the edge-chord of edge  $a'b'$ .

The following terms are defined with respect to given  $r_c$  and  $r_s$ , which satisfy  $r_c < 2r_s$ .

**Definition 4:** Standard Chord: The common chord between two intersecting sensing disks is called a standard chord if the distance between the two sensors is equal to  $r_c$ , the communication range.

**Definition 5:** Long Chord: If the common chord between two intersecting sensing disks is longer than their standard chord, it is called a long chord. (The distance between the two sensors is smaller than  $r_c$ .)

**Definition 6:** Connection Chord: A connection chord is either a long chord or a standard chord. (The distance between the two sensors is smaller than or equal to  $r_c$ .)

If two sensing disks have a connection common chord, then the two sensors can communicate directly with each other, i.e., they are connected by an edge in the sensors' communication network — thus the name *connection* chord.

**Definition 7:** Short Chord: If the common chord between two intersecting sensing disks is shorter than their standard chord, it is called a short chord. (The distance between the two sensors is greater than  $r_c$ .)

If two sensing disks have a short common chord, then the two sensors can *not* communicate directly with each other; they are *not* connected by an edge in the sensors' communication network.

**Definition 8:** Standard Angle  $\theta$ : The angles corresponding to a standard chord at the centers of two sensing disks are called standard angles.  $\theta = 2 \arccos(r_c/2r_s)$ .

Fig. 3 illustrates the above definitions. The polygons referred to in the following definitions are not necessarily Voronoi polygons; and again the definition are made relative to a given  $r_c$  and  $r_s$ .

**Definition 9:** Regular Connection Polygon: a polygon that can be inscribed in a sensing disk, with all its edges of equal length and no shorter than a standard chord.

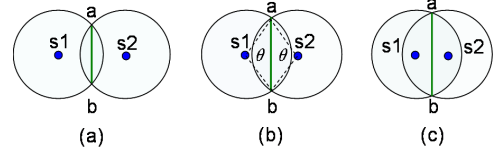


Fig. 3. Let  $D$  denote the distance between two sensors and assume  $r_c < 2r_s$ . (a)  $ab$  is a short chord when  $r_c < D < 2r_s$ ; (b)  $ab$  is a standard chord when  $r_c = D$ .  $\theta$  is the standard angle; (c)  $ab$  is a long chord when  $D < r_c$ . The common chords  $ab$  in (b) and (c) are connection chords.

**Definition 10:** Semi-regular Connection Polygon: a polygon with  $k \geq 4$  sides that can be inscribed in a sensing disk, with four edges each of the length of a standard chord, and the remaining  $k - 4$  edges being of equal length.

**Definition 11:** Reference Polygon: It is either a regular connection polygon or a semi-regular connection polygon.

### III. OPTIMAL PATTERN EXPLORATION

In this section, we describe our journey of exploration for an optimal sensor deployment pattern that provides four-connectivity and full coverage.

#### A. Theoretical Foundation

In our journey, we think of a sensor deployment as a collection of Voronoi polygons, which form a tessellation over a region. There are several benefits by employing Voronoi polygons. First, as the Voronoi polygons form a tessellation, we can regard each Voronoi polygon as the corresponding sensor's effective contribution to coverage. If all Voronoi polygons are of the same size, say  $A$ , then the number of sensors needed to cover a region of area  $R$  is approximately  $R/A$ . We can estimate the number of sensors needed by measuring the average size of each Voronoi polygon. Second, polygon tessellation has been extensively studied. Thinking in terms of Voronoi polygons, we are more able to benefit from the rich literature of polygon tessellations.

Consider a rectangle of area  $R$ , over which we wish to deploy sensors. For a sensor deployment  $d$  over  $R$  that achieves four-connectivity and full-coverage, let  $G_d$  denote the set of Voronoi polygons generated by the sensors. Let  $\mathcal{G}_d$  be the collection of all possible  $G_d$ 's. (Each element in  $\mathcal{G}_d$  is a set of Voronoi polygons.) Our goal is to find a  $G_d \in \mathcal{G}_d$  with the smallest  $|G_d|$ , where  $|G_d|$  denotes the cardinality of  $G_d$ . We denote the smallest  $|G_d|$  by  $C_{\min}$ .

It is difficult to directly search  $\mathcal{G}_d$  for a certain element, since we lack knowledge of this set. Therefore, we will construct another set  $\mathcal{G}_r$  (to be described soon) satisfying the following condition: for any  $G_d \in \mathcal{G}_d$ , there exists a  $G_r \in \mathcal{G}_r$  such that  $|G_d| = |G_r|$ . With this set, we have

$$\min\{|G_d| : G_d \in \mathcal{G}_d\} \geq \min\{|G_r| : G_r \in \mathcal{G}_r\} = C_{\min}. \quad (1)$$

If we can find a  $G_d \in \mathcal{G}_d$  such that  $|G_d| = C_{\min}$ , then that  $G_d$  has the smallest cardinality in  $\mathcal{G}_d$ , and we will have found an optimal deployment pattern.

To construct the aforementioned  $\mathcal{G}_r$ , we first state a basic result, which can be easily proved using a well-known Euler formula. In order not to interrupt the presentation of our main ideas, we defer the lemma's proof to the Appendix.

*Lemma 1:* Let  $\Gamma$  denote a tessellation over a fixed region consisting of  $F$  polygons. If each vertex of  $\Gamma$ , except those at the corner, is on at least three edges, then the average number of sides of the polygons of  $\Gamma$  is not larger than six when  $F$  approaches  $\infty$ .

Lemma 1 indicates that, when sensors are deployed to achieve full coverage over a rectangular region, the average number of edges of the Voronoi polygons generated by them are asymptotically less than or equal to six. Note that Lemma 1 is not a known result. The known property that average number of edges of a Voronoi region is less than 6 only holds for a bounded region, while Lemma 1 in this paper presents the conclusion that holds *asymptotically*. Even though the bound six is only an asymptotical one, when constructing  $\mathcal{G}_r$  we use Lemma 1 as a heuristic and confine ourselves to those sets of polygons whose average number of edges is no more than six.

Based on Lemma 1 and the deployment requirement of full-coverage and four-connectivity, we denote by  $G_r$  any set of polygons that satisfies the following conditions: (1) the average edge number of polygons is not larger than six; (2) each polygon is a reference polygon; (3)  $\sum_{P \in G_r} \text{area}(P) \geq R$ , where  $\text{area}(P)$  denote the area of polygon  $P$ . (Note that the polygons in  $G_r$  are not necessarily the Voronoi polygons of a sensor deployment. As a matter of fact, they don't even have to form a tessellation.)

Let  $\mathcal{G}_r$  denote the set of all such  $G_r$ 's. The following lemma indicates that when  $r_c/r_s > \sqrt{2}$  it is possible to "embed"  $\mathcal{G}_d$  in  $\mathcal{G}_r$ , so that (1) holds. We will present the proof in the Appendix. (Unfortunately, we are unable to prove the same result for the case where  $r_c/r_s \leq \sqrt{2}$ . We will discuss this case in Section IV.)

*Lemma 2:* If  $r_c/r_s > \sqrt{2}$ , then for any  $G_d \in \mathcal{G}_d$  there exists a  $G_r \in \mathcal{G}_r$  such that  $|G_r| = |G_d|$ .

We next establish a lower bound on  $|G_r|$  for any  $G_r \in \mathcal{G}_r$ . This bound must also be a lower bound on  $|G_d|$  for any  $G_d$  in  $\mathcal{G}_d$ , owing to Lemma 2.

*Lemma 3:* If  $r_c/r_s > \sqrt{2}$ , then for any set  $G_r \in \mathcal{G}_r$ ,

$$|G_r| \geq R / (2 \sin \varphi + \sin(2\varphi)) r_s^2,$$

where  $\varphi = \max(\pi/3, \theta)$  and  $\theta$  is the standard angle.

Once again we defer the proof for Lemma 3 to the Appendix.

We comment that the lower bound on  $|G_r|$  is obtained from  $R$  divided by the maximum average coverage contribution of each individual sensor. This lower bound does not tell us a specific deployment. Nevertheless, we can use it to judge if a given deployment is optimal or not. If there is a deployment that provides four-connectivity and full-coverage, and the number of sensors used is equal to this lower bound, this deployment is optimal.

## B. The Diamond Pattern

In the following, we present an optimal deployment pattern called the Diamond pattern when  $r_c/r_s > \sqrt{2}$ .

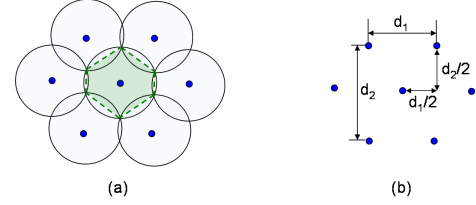


Fig. 4. The Diamond pattern to achieve full coverage and four connectivity where  $r_c/r_s > \sqrt{2}$ . The coverage contribution of each individual sensor is denoted by shaded hexagon.

The Diamond pattern is shown in Fig. 4. The Voronoi polygon generated by each sensor, shown in Fig. 4(a), is six-sided reference polygon. As  $r_c/r_s$  increases from  $\sqrt{2}$ , the length of long chords will decrease while the length of short chords will increase. When  $r_c/r_s = \sqrt{3}$  this polygon becomes a regular hexagon. The shape will not change as  $r_c/r_s$  further increases. Fig. 4(b) illustrates the relative positions of sensors in this pattern,

$$d_1 = 2r_s \cos \frac{\varphi}{2} \sqrt{2(1 - \cos \varphi)}, \quad (2)$$

$$\text{and } d_2 = 2r_s \cos \frac{\varphi}{2} \sqrt{2(1 + \cos \varphi)}, \quad (3)$$

where  $\varphi = \max(2 \arccos(r_c/2r_s), \pi/3)$ . In this pattern, the coverage contribution of each individual sensor is  $d_1 d_2 / 2$ .

Note we use  $d_1$  and  $d_2$  to describe the positions of sensors in this deployment to provide convenience in practical sense. Though the Diamond pattern may look complicated, we can ease our real deployment by taking two steps. We first deploy sensors at the end-points of each grid using  $d_1$  and  $d_2$ , and finally deploy a sensor at the center of the each grid.

*Theorem 1:* The Diamond pattern is the asymptotically optimal deployment pattern to achieve four connectivity and full coverage when  $r_c/r_s > \sqrt{2}$ .

*Proof:* From Definition 8,  $\theta = 2 \arccos(r_c/2r_s)$ . When  $\sqrt{3} \geq r_c/r_s > \sqrt{2}$ , the Voronoi polygon generated by each sensor in the Diamond pattern is a six-sided semi-regular connection polygon. And we have  $\pi/2 > \theta \geq \pi/3$ . Form (2) and (3), we obtain  $d_1 = 2r_s \cos(\theta/2) \sqrt{2(1 - \cos \theta)}$  and  $d_2 = 2r_s \cos(\theta/2) \sqrt{2(1 + \cos \theta)}$ .

Then the area of such a semi-regular hexagon is

$$\begin{aligned} A_1 &= d_1 d_2 / 2 = 4 \cos^2(\theta/2) \sin \theta r_s^2 \\ &= 2(1 + \cos \theta) \sin \theta r_s^2 \\ &= (2 \sin \theta + \sin(2\theta)) r_s^2. \end{aligned}$$

When the Diamond pattern is used to cover a large area  $R$  where the boundary condition can be ignored, the number of such six-sided semi-regular connection polygons needed is

$$N_1 = R / A_1 = R / (2 \sin \theta + \sin(2\theta)) r_s^2. \quad (4)$$

Similarly, when  $r_c/r_s \geq \sqrt{3}$ , the Diamond pattern becomes the regular triangle pattern where the Voronoi polygon generated by each sensor is a six-sided regular connection polygon. We have  $2 \arccos(r_c/2r_s) \leq \pi/3$ . Form (2) and (3), we obtain  $d_1 = \sqrt{3}r_s$  and  $d_2 = 3r_s$ .

In this case, the area of such a regular hexagon is

$$A_2 = d_1 d_2 / 2 = 3\sqrt{3}r_s^2 / 2. \quad (5)$$

When the Diamond pattern is used to cover a large area  $R$  where the boundary condition can be ignored, the number of such six-sided regular connection polygons needed is

$$N_2 = R/A_2 = 2\sqrt{3}R/9r_s^2 = R/(2 \sin \frac{\pi}{3} + \sin \frac{2\pi}{3})r_s^2. \quad (6)$$

Equations (4) and (6) can be re-written as

$$R/(2 \sin \varphi + \sin(2\varphi))r_s^2, \quad (7)$$

where  $\varphi = \max(2 \arccos(r_c/2r_s), \pi/3)$ , which is the exactly the lower bound stated in Lemma 3. ■

#### IV. PATTERN EVOLUTION

We have shown the Diamond pattern to be asymptotically optimal when  $r_c/r_s > \sqrt{2}$ . In this section, we investigate the case where  $r_c/r_s \leq \sqrt{2}$ . As will become clear shortly, the Square pattern can be viewed as a degenerated Diamond pattern.

The Square pattern can be easily described using a diagram. Fig. 5 shows such a diagram, where  $d_1 = d_2 = \sqrt{2}r_c$ . By rotating the diagram in Fig. 5 for 45 degrees, we obtain Fig. 6, in which it is easy to see that each Voronoi polygon is a square, with  $d'_1 = d'_2 = r_c$ . The effective contribution of each individual sensor to coverage is therefore

$$A_S = d'_1 d'_2 = r_c^2. \quad (8)$$

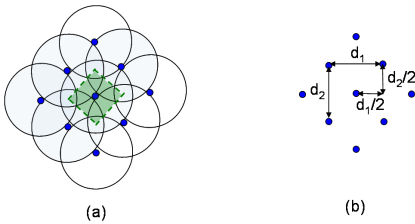


Fig. 5. The Square pattern to achieve full coverage and four connectivity when  $r_c/r_s \leq \sqrt{2}$ . The coverage contribution of each individual sensor is denoted by a shaded square.

We display the Diamond pattern and the Square pattern together in Fig. 7, in an attempt to see their relationship. The figure actually shows the Voronoi polygons corresponding to various patterns rather than the patterns themselves. To see how these Voronoi polygons evolve as  $r_c/r_s$  changes value, let us assume that the sensing range  $r_s$  is fixed, and the communication range  $r_c$  goes from large to small. When  $r_c$  is sufficiently large so that  $r_c/r_s \geq \sqrt{3}$ , the regular Diamond pattern, whose Voronoi polygons are regular connection hexagons

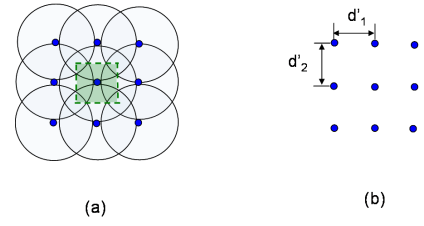


Fig. 6. Another view of the Square pattern.

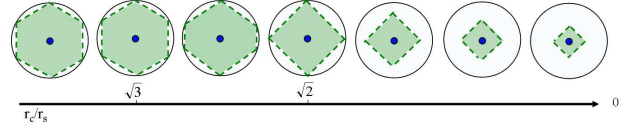


Fig. 7. The Voronoi polygon generated in different deployment patterns is shown with dashed line segments. The amount of coverage contribution of each individual sensor is denoted by the shaded area.

(as defined in Definition 9), is optimal. As  $r_c$  gets smaller, in order to maintain four-connectivity of the network, some sensors need to get closer to each other. As we have proved in Theorem 1 and depicted in Fig. 7, the semi-regular Diamond pattern, whose Voronoi polygons are semi-regular connection hexagons (as defined in Definition 10), is still optimal for the case where  $\sqrt{3} > r_c/r_s > \sqrt{2}$ .

If we let the semi-regular connection hexagon continue to shrink, it becomes a square when  $r_c/r_s = \sqrt{2}$ . The square gets smaller and smaller as  $r_c/r_s$  continues to decrease. An interesting question arises: Is the Square pattern optimal for  $r_c/r_s \leq \sqrt{2}$ ? We conjecture that the answer is positive. Its proving (or disproving), we believe, is an interesting open problem. It is part of our future work.

#### V. NUMERICAL RESULTS

In this section, we compare the numbers of nodes needed for various patterns to provide both four connectivity and coverage over a deployment region of size  $1000m \times 1000m$  with  $r_s = 30m$ , and  $9m < r_c \leq 54m$ , i.e.,  $r_c/r_s$  varies from 0.3 to 1.8.

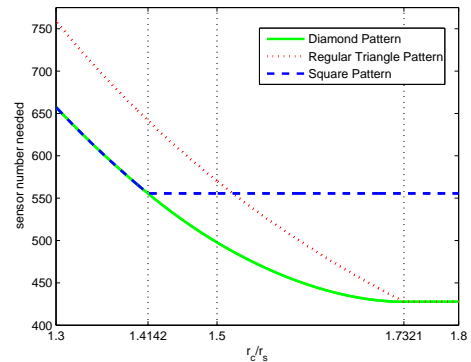


Fig. 8. Numbers of nodes needed to achieve four connectivity and full coverage.  $r_c/r_s$  varies from 1.3 to 1.8.

In Fig. 8, we compare the performances of three patterns — the Diamond pattern, the regular triangle lattice pattern, and the Square pattern — with  $r_c/r_s$  varying from 1.3 to 1.8 ( $r_c$  changing from 39m to 54m). We make the following observations:

- 1) It is convenient to view the Diamond pattern as a series of transiting patterns as shown in Fig. 7. As such, the Diamond pattern coincides with the Square pattern when  $r_c/r_s$  is small. At  $r_c/r_s = \sqrt{2}$ , i.e., 1.4142, the two patterns diverge. Afterwards, the Diamond pattern stands alone until  $r_c/r_s = \sqrt{3}$ , i.e., 1.7321, when it converges with the regular triangle lattice pattern.
- 2) The Diamond pattern outperforms the regular triangle lattice pattern when they are separate (i.e., when  $r_c/r_s < \sqrt{3}$ ). For instance, compared with the regular triangle lattice pattern, the Diamond pattern can save about 13.7% of nodes when  $r_c/r_s = 1.5$ , and 14.9% when  $r_c/r_s = \sqrt{2}$ .
- 3) Also, the Diamond pattern outperforms the Square pattern when the two are separate. The Square pattern costs 11.6% more sensors when  $r_c/r_s = 1.5$ , and costs 25% more when  $r_c/r_s = \sqrt{3}$ , compared with the Diamond pattern. This difference keeps unchanged as  $r_c/r_s$  further increases.

## VI. REMARKS ON SENSING AND COMMUNICATION MODELS

In this section, we briefly discuss various sensing and communication models that have been proposed in the literature, and then comment on the particular model adopted in this paper.

It is suggested that, the capability of sensing could gradually attenuate with increasing distances. In [10], Megerian *et al.* present a model for sensing sensitivity. In their model, the sensing sensitivity decreases exponentially with increasing target distance. Cao *et al.* in [3] suggest the sensing range of passive infrared (PIR) sensor roughly follows two-dimensional Gaussian. Zhou and Chakrabarty in [16] propose a probabilistic sensing model containing three different ring-shaped areas. The target can be detected with probability 1 in the first area, with probability less than 1 but larger than 0 in the second area, and with probability 0 in the third area. These models reflect the fact that sensing disk boundary could not be determined accurately.

Studies have also suggested that wireless communication links could be irregular and non-isotropic. In some applications, disruptive physical phenomena may need to be considered. Zuniga and Krishnamachari in [17] identify the causes of the transitional region in low power wireless communication links, and use the techniques from information theories to quantify their influence. Based on those, the log-normal shadowing model is proposed. In [15], Zhou *et al.* propose the radio irregularity model (RIM). Based on experimental data, RIM takes into account both the non-isotropic properties of the propagation media and the heterogeneous properties of

devices. In [11], Moscibroda *et al.* propose the SINR model. In this model, propagation channel properties are so important such that a node may not be able to receive messages correctly even if it is close to the sender. Generally, realistic modeling of communication links between wireless sensing devices is challenging, and link parameters often vary in different deploy environments and hardware specifications.

We use the disk model in this paper. Reflecting the ideal case, the disk model can be considered a clean abstraction ignoring any uncertain physical disruptiveness. Abstraction is inevitable to achieve enough generality while aiming to lay down the certain theoretical foundations. The disk model can also be considered as a conservative measure. For instance, we can set a conservative threshold to get  $r_s$  in the probabilistic sensing cases, and we can get a conservative  $r_c$  by taking the lower bound in the non-isotropic communication cases. Exploring optimal deployment patterns for the sensors with non-disc sensing and communication models is valuable. We believe that the methodology and results presented in this paper based on the disk model would act as cornerstones for future research.

## VII. CONCLUSIONS

This work is the first to study optimal deployment patterns for full coverage and four connectivity. We proposed a Diamond pattern, which can be viewed as a series of evolving patterns. When  $r_c/r_s \geq \sqrt{3}$ , the Diamond pattern coincides with the well-known triangle lattice pattern; when  $r_c/r_s \leq \sqrt{2}$ , it degenerates to the Square pattern. We proved the Diamond pattern to be asymptotically optimal when  $r_c/r_s > \sqrt{2}$ . It is challenging to search for optimal deployment patterns in wireless sensor networks. We hope our work can shed some insights on further exploration to this regard.

## REFERENCES

- [1] A. Arora, et. al. ExScal: Elements of an Extreme Scale Wireless Sensor Network. In *IEEE International Conference on Real-Time Computing Systems and Applications (RTCSA)*, Hong Kong, 2005.
- [2] X. Bai, S. Kumer, D. Xuan, Z. Yun and T. H. Lai. Deploying wireless sensors to achieve both coverage and connectivity. In *Proceedings of ACM Annual International Symposium on Mobile Ad-Hoc Networking and Computing (MobiHoc)*, pages 131-142, Florence, Italy, 2006.
- [3] Q. Cao, T. Yan, J. Stankovic, and T. Abdelzaher. Analysis of Target Detection Performance for Wireless Sensor Networks. In *IEEE International Conference on Distributed Computing in Sensor Networks (DCOSS)*, Marina del Rey, CA, 2005.
- [4] G. Dimakis. Codes on Graphs for Distributed Storage in Wireless Networks. [http://www.eecs.berkeley.edu/adim/MS\\_Thesis.pdf](http://www.eecs.berkeley.edu/adim/MS_Thesis.pdf), EECS Master Degree Thesis, Unveristy of California at Berkeley, 2005.
- [5] M. Goyeneche and J. Villadangos and J. Astrain and M. Prieto and A. Cordoba. A Distributed Data Gathering Algorithm for Wireless Sensor Networks with Uniform Architecture. In *Proceedings of IEEE EUROMICRO International Conference on Parallel, Distributed and Network-Based Processing (PDP)*, Vol. 0, pages 373-380, Naples, Italy, 2007.
- [6] F. Hillier and G. Lieberman. *Introduction to Operations Research*. McGraw-Hill, 2002.
- [7] R. Iyengar, K. Kar and S. Banerjee. Low-coordination Topologies for Redundancy in Sensor Networks. In *Proceedings of ACM Annual International Symposium on Mobile Ad-Hoc Networking and Computing (MobiHoc)*, pages 332-342, Urbana-Champaign, IL, 2005.

- [8] R. Kershner. The Number of Circles Covering a Set. *American Journal of Mathematics*, Vol. 61, pages 665-671, 1939.
- [9] A. Panangadan and G. Sukhatme. Data Segmentation for Region Detection in a Sensor Network. [http://cres.usc.edu/cgi-bin/print\\_pub\\_details.pl?pubid=434](http://cres.usc.edu/cgi-bin/print_pub_details.pl?pubid=434), CRES Technical Report 05-005, Univeristy of Southern California, 2005.
- [10] S. Megerian, F. Koushanfar, G. Qu, G. Veltri, and M. Potkonjak, Exposure in Wireless Sensor Networks: Theory and Practical Solutions, *Wireless Networks*, v.8(5), pp. 443-454, 2002.
- [11] T. Moscibroda, R. Wattenhofer and A. Zollinger, Topology Control Meets SINR: The Scheduling Complexity of Arbitrary Topologies, In Proceedings of *ACM Annual International Symposium on Mobile Ad-Hoc Networking and Computing (MobiHoc)*, pages 131-142, Florence, Italy, 2006.
- [12] Y. Wang, C. Hu, and Y. Tseng. Efficient Deployment Algorithms for Ensuring Coverage and Connectivity of Wireless Sensor Networks. In *Wireless International Conference (WICON)*, Budapest, Hungary, 2005.
- [13] H. Zhang and J. Hou. Maintaining Sensing Coverage and Connectivity in Large Sensor Networks. In *NSF International Workshop on Theoretical and Algorithmic Aspects of Sensor, Ad Hoc Wirelsss, and Peer-to-Peer Networks*, 2004.
- [14] J. Zhao and R. Govindan. Understanding Packet Delivery Performance in Dense Wireless Sensor Networks. In Proceedings of *ACM Conference on Embedded Networked Sensor Systems (SenSys)*, pages 1-13, Los Angeles, CA, 2003.
- [15] G. Zhou, T. He, S. Krishnamurthy, and J. Stankovic. Impact of Radio Irregularity on Wireless Sensor Networks. In Proceedings of *ACM International Conference on Mobile Systems, Applications, and Services (MobiSys)*, pages 125-138, Boston, MA, 2004.
- [16] Y. Zhou and K. Chakrabarty, Sensor Deployment and Target Localization Based on Virtual Force, In Proceedings of *Annual Conference of the IEEE Computer Communications (InfoCom)* pp. 1293-1303, 2003.
- [17] M. Zuniga and B. Krishnamachari, Analyzing the Transitional Region in Low Power Wireless Links, In Proceedings of *Annual IEEE Communication Society Conference on Sensor, Mesh and Ad Hoc Communications and Networks (SECON)* pp. 517-526, 2004.

## APPENDIX

### A. Proof of Lemma 1

*Proof:* The proof technique here is inspired by [8]. Let  $V$  denote the number of vertices and  $E$  denote the number of edges in the tessellation  $\Gamma$ . Let  $C$  denote the number of corners, which is a constant for a fixed region. Since each vertex except for those at corners is on at least three edges and each edge is on two vertices, we have

$$3V - C \leq 2E. \quad (9)$$

We also have the Euler relation for  $\Gamma$ :

$$V - E + F = 1.$$

Substituting (9) into the Euler relation for  $\Gamma$ , we obtain

$$E \leq 3F - 3 + C.$$

Now let  $e_i$  ( $i = 1, 2, \dots, F$ ) denote the number of edges on the  $i$ th polygon. Let  $B$  denote the number of boundary edges, which are on only one polygon. Since all other edges are each on two polygons, we have

$$\sum_{i=1}^F e_i \leq \sum_{i=1}^F e_i + B = 2E \leq 6F - 6 + 2C. \quad (10)$$

Dividing  $F$  into Eq. 10 yields

$$\frac{1}{F} \sum_{i=1}^F e_i \leq 6 - \frac{6}{F} + \frac{2C}{F},$$

the right side of which equals 6 as  $F$  approaches  $\infty$ .

Note that, when  $F$  is finite  $(1/F) \sum_{i=1}^F e_i \leq 6$  may not hold; it depends on  $C$ . ■

### B. Proof for Lemma 2

*Proof:* We prove this Lemma by carrying out transformations from any given  $G_d$  to a  $G_r \in \mathcal{G}_r$ .

Since each polygon in  $G_d$  is a Voronoi polygon generated by a sensor, each edge of them must reside on one common chord between two sensing disks as shown in Fig. 2. This chord is called an edge-chord. The transformation is carried out on these edge-chords such that the polygons are changed to desired shapes.

Since we are looking for a  $G_r \in \mathcal{G}_r$ , transformation is only allowed if the following three constraints are all satisfied. First, the total area of the polygons in  $G_r$  will be larger than or equal to the total area of  $G_d$ ; second, the average number of edges of polygons in  $G_r$  is not larger than six; third, each polygon in  $G_r$  has at least four edge-chords that are connection chords. The above three constraints together guarantee that  $G_r$  obtained after transformation be in the set  $\mathcal{G}_r$ .

Considering one  $k$ -sided polygon in  $G_d$ , if  $2\pi/k \geq \theta$  where  $\theta$  is the standard angle as defined in Definition 8, we transform this polygon to a  $k$ -sided regular connection polygon as defined in Definition 9 by letting each edge be overlapped totally with its edge-chord and of the same length. After transformation, the area will not decrease since the regular polygon has the maximum area when  $k$  is given, which can be proved using Lagrangian multipliers [6]. At the same time, four connectivity will not be violated. Since the number of edges is not changed, the average edge number of polygons will not change.

Now we consider the case where  $2\pi/k < \theta$ . First, if among  $k$  edge-chords there are more than four connection chords, we randomly delete some of them to let only four be left, and add one short chord when necessary. Fig. 9 illustrates this transformation. Then, if among the four connection chords

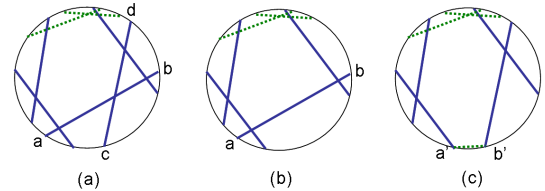


Fig. 9. The large circle denotes the sensing disk. The solid lines denote the connection chords. The dashed lines denote the short chords. (a) The polygon in  $G_d$  before transformation; (b) If we remove the connection chord  $cd$ , no short chord needed to add; (c) If we remove the connection chord  $ab$ , a short chord  $a'b'$  is needed to connect the “open side” that results from the removing in the circumference.

there are some long chords, we change them into standard

chords. The transformation is made by fixing one end point of these long chords and rotating them toward outside until they become standard chords. Fig. 10 illustrates this step. Next, we

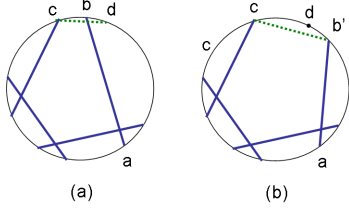


Fig. 10. The large circle denotes the sensing disk. The solid lines denote the connection chords. The dashed lines denote the short chords. (a) The polygon before transformation; (b) Rotate long chord  $ab$  towards outside until it becomes a standard chord  $ab'$ . We let short chord meet  $ab$  at the circumference when necessary.

shift standard chords along the circumference until not any two standard chords intersect each other within the sensing disk. Then use  $k-4$  short chords together with four standard chords to construct a polygon with vertices all on the circumference. The purpose of this step is to make the overlapped area among any three sensing disks to be as small as possible. This transformation is always feasible since  $r_c/r_s > \sqrt{2}$ . Fig. 11 illustrates this transformation. Finally, we transform polygons

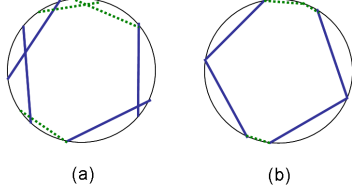


Fig. 11. The large circle denotes the sensing disk. The solid lines denote the connection chords. The dashed lines denote the short chords. (a) The polygon before transformation; (b) Shift standard chords such that there are no standard chords intersecting each other within the sensing disk. Connect their ends with three short chords.

into semi-regular connection polygon as defined in Definition 10 by shifting standard chords along the circumference and letting short chords equally share the remaining arc. Since  $r_c/r_s > \sqrt{2}$ , the angle made at the center of the sensing disk by the remaining arc is always larger than 0. Fig. 12 illustrates this final transformation.

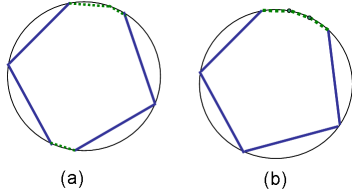


Fig. 12. The large circle denotes the sensing disk. The solid lines denote the connection chords. The dashed lines denote the short chords. (a) The polygon before transformation; (b) Shift standard chords such that all standard chords are together. Let three short chords equally share the left arc.

Now we denote the set of polygons after transformation as  $G_r$ .  $G_r$  consists of only reference polygons and  $G_r = G_d$ .

As we can see from the transformation procedure, transformations do not decrease total area of polygons. Also they do not increase the edge number since only deleting chords are allowed. They further do not violate the condition that at least four edge-chords of each polygon are connection chords. Hence,  $G_r \in \mathcal{G}_r$ . ■

### C. Proof for Lemma 3

Let  $M_k$  ( $k \geq 5$ ) denote the area of a polygon in  $G_r$ , which is the set of reference polygons after the transformations in Lemma 2. We have

$$M_k = 2r_s^2 \sin \varphi + \frac{(k-4)r_s^2}{2} \sin \frac{2\pi - 4\varphi}{k-4}, \quad (11)$$

where  $\varphi = \max(2\pi/k, \theta)$ . Recall that  $\theta$  is the standard angle as defined in Definition 8,  $\theta = 2 \arccos(r_c/2r_s)$ .

To prove Lemma 3, we need to first prove the following lemma.

*Lemma 4:* For  $k \geq 5$ ,

$$0 < M_{k+1} - M_k < M_k - M_{k-1}. \quad (12)$$

*Proof:* It can be proved by extensively using Taylor's expansion for  $\sin x$ .

Let  $f(k)$  is defined as  $f(k) = M_{k+1} - M_k$ . The proof can be divided into the following four cases.

Case 1: When  $\varphi \leq 2\pi/(k+1)$ ,  $M_{k+1}$ ,  $M_k$  and  $M_{k-1}$  are the areas of the regular connection polygons. Therefore, at this time, the claim that " $f(k) > 0$  and  $f(k)$  is decreasing as  $k$  increases" follows directly from Lemma 2 of [8] (Lemma 2 in [8] states that, the area of regular polygons will increase as the number of edges increases. But the amount of area increment will decrease as the number of edges increases).

Case 2: When  $\varphi \geq 2\pi/(k-1)$ ,  $M_{k+1}$ ,  $M_k$  and  $M_{k-1}$  are the areas of the semi-regular connection polygons. This case essentially has no difference from case 1, since the polygons are of the same type. Hence, exactly the same technique used in proof of Lemma 2 in [8] can show the claim holds at this time.

The first inequality in (12) can be easily proved using Taylor's expansion for  $\sin x$ . We now prove the second inequality. we have

$$\begin{aligned} f(k) &= \frac{(k-3)r_s^2}{2} \sin \frac{2\pi - 4\varphi}{k-3} \\ &\quad - \frac{(k-4)r_s^2}{2} \sin \frac{2\pi - 4\varphi}{k-4}. \end{aligned}$$

Taking derivatives of both sides of the above equation, we get

$$\begin{aligned} \frac{df(k)}{dk} &= \frac{r_s^2}{2} \left[ \sin \frac{2\pi - 4\varphi}{k-3} - \frac{2\pi - 4\varphi}{k-3} \cos \frac{2\pi - 4\varphi}{k-3} \right] \\ &\quad - \frac{r_s^2}{2} \left[ \sin \frac{2\pi - 4\varphi}{k-4} - \frac{2\pi - 4\varphi}{k-4} \cos \frac{2\pi - 4\varphi}{k-4} \right]. \end{aligned}$$

Since  $\sin x - x \cos x$  is an increasing function of  $x$  in  $(0, \pi)$  and  $(2\pi - 4\varphi)/(k-3)$ ,  $(2\pi - 4\varphi)/(k-4) \in (0, \pi)$  for  $k \geq 5$ ,  $df(k)/dk < 0$  for  $k \geq 5$ . Hence,  $f(k)$  is a decreasing function, and thus (12) holds when  $2\pi/(k-1) \leq \varphi$ .

Case 3: When  $2\pi/(k+1) < \varphi \leq 2\pi/k$ , for  $k \geq 4$ , let

$$M_k^r = \frac{r_s^2}{2} k \sin \frac{2\pi}{k}$$

and

$$M_k^s = 2r_s^2 \sin \varphi + \frac{r_s^2(k-4)}{2} \sin \frac{2\pi-4\varphi}{k-4}.$$

Then,  $M_{k+1} = M_{k+1}^s$ ,  $M_k = M_k^r$ , and  $M_{k-1} = M_{k-1}^r$ . To show at this time  $f(k) > 0$ , we have

$$\begin{aligned} M_{k+1}^s - M_k^r &= \frac{(k-3)r_s^2}{2} \sin \frac{2\pi-4\varphi}{k-3} \\ &+ r_s^2 \sin \varphi - \frac{kr_s^2}{2} \sin \frac{2\pi}{k}, \end{aligned}$$

which is greater than 0 for  $2\pi/(k+1) < \varphi \leq 2\pi/k$ .

For the claim that  $f(k)$  is decreasing as  $k$  increases in this case, we need to prove  $M_{k+1}^s - M_k^r < M_k^r - M_{k-1}^r$ , which follows from the conclusion for the case 2 and the fact that  $M_{k+1}^s < M_{k+1}^r$ . The latter inequality holds since  $M_{k+1}^s$  is the maximum area possible of any  $(k+1)$ -sided polygon inscribed in a sensing disk.

Case 4: When  $2\pi/k < \varphi < 2\pi/(k-1)$ , for the claim that  $f(k) > 0$ , we notice  $0 < M_{k+1}^s - M_k^s$  is obvious. For the claim that  $f(k)$  is decreasing as  $k$  increases in this case, we need to prove  $M_{k+1}^s - M_k^s < M_k^s - M_{k-1}^r$ , which follows by note that

$$\begin{aligned} &(M_k^s - M_{k-1}^r) - (M_{k+1}^s - M_k^s) \\ &= (k-4)r_s^2 \sin \frac{2\pi-4\varphi}{k-4} - \frac{r_s^2}{2}(k-5) \sin \frac{2\pi}{k-5} \\ &- \frac{r_s^2}{2}(k-3) \sin \frac{2\pi-4\varphi}{k-3} \end{aligned}$$

is greater than 0 when  $2\pi/k < \varphi < 2\pi/(k-1)$  by using Taylor's expansion for  $\sin x$ .

The four cases together prove that  $f(k) > 0$  and  $f(k)$  is decreasing as  $k$  increases for all values of  $\varphi$ , where  $f(k)$  is defined as  $f(k) = M_k - M_{k-1}$ , where  $M_k$  is expressed in (11) and  $k \geq 5$ . ■

Now we are ready to prove Lemma 3.

*Proof:* Let  $n_i$  ( $i = 3, 4, \dots, m$ ) denote the number of polygons in  $G_r$  with  $i$  edges, so we have

$$\sum_{i=3}^m n_i = |G_r|.$$

Since  $G_r \in \mathcal{G}$ , the average number of sides of the polygons of  $G_r$  is smaller than six, i.e.,

$$\sum_{i=3}^m i n_i \leq 6 \sum_{i=3}^m n_i,$$

which can be rewritten as

$$\sum_{i=7}^m (i-6)n_i \leq 5 \sum_{i=3}^m (6-i)n_i.$$

By Lemma 4 that states  $f(k)$  is decreasing as  $k$  increases,

we can strengthen the above as

$$\sum_{i=7}^m (i-6)(M_7 - M_6)n_i \leq \sum_{i=3}^5 (6-i)(M_6 - M_5)n_i. \quad (13)$$

The fact that  $f(k)$  is decreasing as  $k$  increases implies that the interval from  $M_q$  to  $M_p$  consists of  $(p-q)$  subintervals among which the shortest is  $M_p - M_{p-1}$  and the longest is  $M_{q+1} - M_q$ .

We then have for  $p > q \geq 5$ ,

$$(p-q)(M_p - M_{p-1}) \leq (M_p - M_q), \quad (14)$$

$$\text{and} \quad (M_p - M_q) \leq (p-q)(M_{q+1} - M_q). \quad (15)$$

Hence, by (14) we have

$$(6-i)(M_6 - M_5) \leq (M_6 - M_i), \quad i < 6 \quad (16)$$

and by (15)

$$M_i - M_6 \leq (i-6)(M_7 - M_6), \quad i > 6. \quad (17)$$

Then from (13), (16) and (17),

$$\sum_{i=3}^m M_i n_i \leq M_6 \sum_{i=3}^m n_i = |G_r| M_6,$$

where  $\sum_{i=3}^m M_i n_i \geq R$ .

We then have  $R \leq |G_r| M_6$ . This concludes our proof. ■